Structural and optical properties of epitaxially overgrown third-order gratings for InGaN/GaN-based distributed feedback lasers

Linda T. Romano,[a] Daniel Hofstetter, Matthew D. McCluskey, David P. Bour, and Michael Kneissl
Xerox Palo Alto Research Center, 3333 Coyote Hill Road, Palo Alto, CA 94304

(Received 7 August 1998; accepted for publication 11 September 1998)

Laser-diode heterostructures of InGaAlN containing a third-order diffraction grating for distributed optical feedback have been examined with transmission electron microscopy (TEM) and scanning electron microscopy (SEM). The grating was defined holographically and etched by chemically assisted ion-beam etching into the upper GaN confinement layer of the laser structure. After the etch step, it was overgrown with an $Al_{0.08}Ga_{0.92}N$ upper cladding layer. Threading dislocations were present that initiated at the sapphire substrate, but no new dislocations were observed at the grating/$Al_{0.08}Ga_{0.92}N$ interface. A comparison of TEM and SEM micrographs reveals that there is a compositional gradient in the AlGaN upper cladding layer; however, calculations show that it did not reduce the optical coupling coefficient of the grating. © *1998 American Institute of Physics.* [S0003-6951(98)04545-8]

Within the last couple of years, research on semiconductor lasers with emission wavelengths around 400 nm has received a great deal of attention. Recent milestones in the development of nitride-based light emitters have been the demonstration of high-brightness blue/green light emitting diodes and both pulsed and continuous-wave laser operation at room temperature.[1–5] Mainly for the purpose of overcoming difficulties in high-quality mirror fabrication, but also in order to improve mode selection and wavelength stability, distributed feedback (DFB) blue lasers have been demonstrated recently.[6] Etching and regrowth of the grating, which typically completes the device structure, is a major obstacle for the fabrication of DFB lasers in material systems other than the nitrides. The strong chemical bonds between gallium and nitrogen result in a very stable and chemically inert surface, compared to GaAs materials for example, where oxides are readily formed on the surface.

In this letter, we present a structural evaluation of a third-order diffraction grating from InGaN/GaN-based DFB lasers. The grating was defined by holography and etched into the GaN upper confinement layer by chemically assisted ion-beam etching (CAIBE). After etching, it was overgrown with an $Al_{0.08}Ga_{0.92}N$ upper cladding layer and a GaN contact layer. We compare scanning electron microscopy (SEM) and transmission electron microscopy (TEM) cross sections of the grating before and after overgrowth. Based on these observations, we estimate how an effective alteration of the grating profile due to a compositional gradient might affect the grating's coupling coefficient and thus the threshold gain of the laser.

The fabrication of these devices relied on growing a 4 μm thick *n*-type GaN:Si layer on *C*-face sapphire. On top of this layer, we grew a 500 nm thick, *n*-type $Al_{0.08}Ga_{0.92}N$:Si lower cladding layer, a 100 nm thick *n*-type GaN:Si lower waveguiding layer, an active region with five 3.5 nm thick $In_{0.1}Ga_{0.9}N$ quantum wells and 9.0 nm thick GaN barriers, and a 180 nm thick *p*-type GaN:Mg upper waveguiding layer. More details about growth conditions and doping levels can be found in Ref. 5. The thicknesses of the layers in the active region were determined by TEM. The third-order grating with a period of 240 nm was then defined by a holographic exposure with a single-mode HeCd laser at an emission wavelength of 325 nm. Next, we transferred the grating into the GaN upper waveguiding layer with CAIBE. The grating depth was approximately 85 nm, which theoretically results in a coupling coefficient of 50–100 cm^{-1} for a rectangular grating. Figure 1 shows an SEM cross section of the grating before regrowth. The tooth shape is a symmetric trapezoid with 70° sidewall angle, a slightly rounded top, and approximately 2:3 line to space ratio. The bottom of the grating looks flat with a slight slope in the areas close to the sidewall, the sloped bottom being an etching artifact. The composition of the lower AlGaN cladding layer was measured by x-ray diffraction (XRD) with the AlGaN (0006) reflection. The position of the peak corresponded to an Al mole fraction of 8.2%, by assuming a relaxed alloy, and had a full width at half maximum (FWHM) of 5.4 arcmin. The width of the AlGaN peak was found to be slightly broader than the width of the GaN (0006) peak (4.9 min), which indicates that either strain or small composition variations are present in the AlGaN layer.

Next, we proceeded with an epitaxial regrowth to complete the device structure. The regrowth consisted of a 250 nm thick *p*-type $Al_{0.08}Ga_{0.92}N$:Mg upper cladding layer and a 100 nm thick *p*-type GaN:Mg contact layer. The rocking

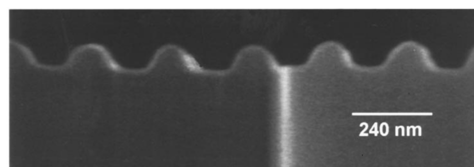

FIG. 1. SEM cross section of a third-order grating fabricated in GaN. The period is 240 nm and the grating depth is 85 nm.

[a]Electronic mail: romano@parc.xerox.com

 © 1998 American Institute of Physics
Downloaded 23 Dec 2005 to 134.121.128.99. Redistribution subject to AIP license or copyright, see http://apl.aip.org/apl/copyright.jsp

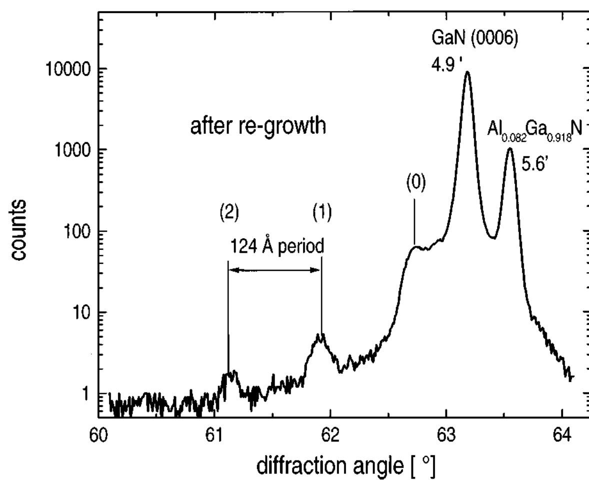

FIG. 2. X-ray diffraction curve measured after regrowth indicating no degradation of the QW multiple superlattice peaks.

curve for the full device structure after overgrowth is presented in Fig. 2. The width of the AlGaN peak (5.6 arcmin) and the position of the peak do not change significantly after the regrowth, which shows that the two AlGaN layers have nearly identical Al content. In addition, no change was observed in the intensity or width of the zeroth-, first-, and second-order superlattice peaks corresponding to the InGaN/GaN multiquantum wells, which indicates that they were structurally similar after regrowth. From the position of the InGaN zeroth-order peak and the period of the superlattice peaks, we obtained a value of 10% In for the InGaN alloy composition of the quantum wells. This value was obtained by taking into account that the InGaN layers are pseudomorphically strained as discussed recently.[7] The period of the superlattice peaks (12.4 nm) in the XRD spectrum corresponds very well to the total well and barrier thickness as determined from TEM.

Cross-sectional TEM images of the overgrown grating, taken near the $\langle 11\underline{2}0\rangle$ zone, are shown in Fig. 3. Dislocations with components of their burgers vectors parallel or perpendicular to the interface are shown in Fig. 3(a) ($g=0002$) and 3(b) ($g=10\underline{1}0$), respectively. The imaging conditions in Fig. 3(a) also show the contrast in the layers due to the difference in atomic number. In this image, the AlGaN, GaN, and multiquantum well layers were identified by both the contrast difference and by x-ray chemical analysis in the TEM. Therefore, the position of the grating could be determined and compared in both of the images. Note the slightly higher magnification (two grating periods) used in Fig. 3(a) to reveal composition details in the region around the grating. The lower magnification image in Fig. 3(b) represents an area that covers four grating periods. In both images, only threading dislocations are observed that initiated at the GaN/substrate interface. No additional dislocations could be found at the interface between the grooved GaN waveguide layer and the upper AlGaN cladding layer. This is very different from overgrowths made with InGaAsP/InP-based infrared DFB lasers, for example, where the grooved interface serves as starting point for numerous dislocations.[8] An additional fringe contrast is observed in the area of the grating [Fig. 3(a)] which will be discussed below.

Although the TEM and SEM specimens were prepared from adjacent areas of the device, the two microscopies revealed a different shape of the grating teeth. In the TEM picture in Fig. 3(a), the grating does not appear flat bottomed. By choosing different imaging conditions, we were able to observe the as-etched grating profile, as indicated by the arrows; but the contrast was very low. On the other hand, there were several fringes with a relatively high contrast above of the grating. As shown in the schematic drawing of Fig. 4, these fringes most likely represent a compositional gradient in the overgrown AlGaN layer. This phenomenon is similar to what has been observed in the growth of AlGaAs/GaAs quantum wire lasers,[9,10] where Ga-rich and Al-rich superlattices spontaneously form along the sidewalls of V-grooves due to the lower surface mobility of Al atoms as compared to Ga atoms. Likewise, we can expect the formation of a Ga-rich AlGaN alloy in the GaN grooves present in our samples. However, as growth proceeds, the surface becomes planar, leading to less severe segregation effects.

Since a compositional gradient could also affect the grating coupling coefficient, κ, we estimated κ from experimental data and compared it with results from a numerical analysis. The following formula is the amplitude equality condition which can be solved for the net threshold gain, γ_{th} (Ref. 11).

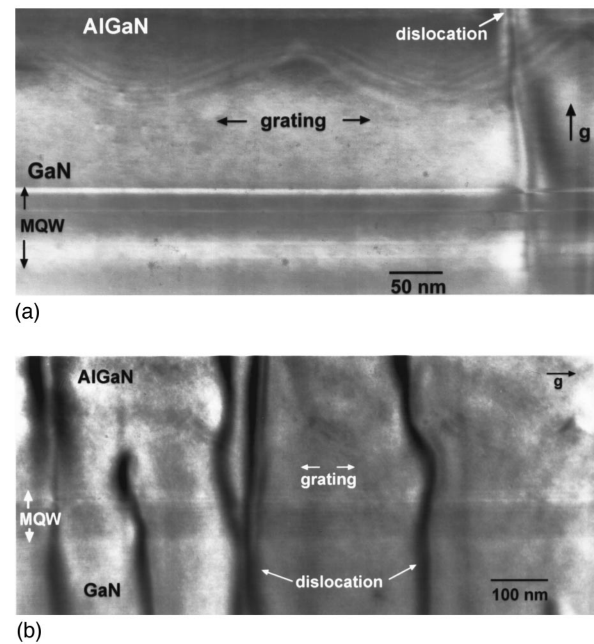

FIG. 3. TEM cross-sectional images of the grating near the ⟨1120⟩ zone direction: (a) $g=0002$ and (b) $g=1010$.

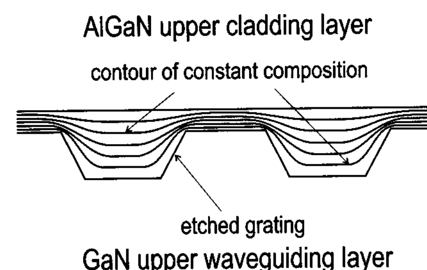

FIG. 4. Schematic picture of the grating after regrowth.

Downloaded 23 Dec 2005 to 134.121.128.99. Redistribution subject to AIP license or copyright, see http://apl.aip.org/apl/copyright.jsp

$$\frac{e^{2\gamma_{th}L}}{(\gamma_{th})^2+\left[\frac{(m+0.5)\pi}{L}\right]^2}=\left(\frac{2}{\kappa}\right)^2. \quad (1)$$

This formula describes the relation between net threshold gain, coupling coefficient, κ, and cavity length, L. The parameter m is the order of the mode and usually can be set at $m=0$. The experimental value for κ was determined specifically by comparing threshold current densities of DFB lasers with different cavity lengths and assuming an absorption and scattering loss value which was measured independently on a set of Fabry–Perot lasers with different cavity lengths and mirror coatings.[12,13] From this measurement, we found that the total scattering and absorption loss is on the order of 40–50 cm^{-1}. This number was added to the net threshold gain in order to obtain threshold gain values. Further assuming a linear relationship between optical gain and current density allowed us to fit threshold current densities of DFB lasers as a function of inverse cavity length with the coupling coefficient being a fit parameter. This procedure yielded $\kappa=4-8\ cm^{-1}$.

The numerical analysis is based on Ref. 10 as well; it takes into account the shape of the grating teeth and the overlap of the optical mode with the grating layer according to the formula

$$\kappa=\frac{i\omega\epsilon_0 a_l}{4}\int_{-\infty}^{\infty}\Delta n^2(x)[E_y(x)]^2dx \quad (2)$$

which contains the effective index difference of the corrugated interface, $\Delta n^2(x)$. For flat-bottomed gratings, $\Delta n^2(x)$ is defined via

$$\Delta n^2(x)=\begin{cases} n_{GaN}^2-n_{AlGaN}^2 & \text{tooth area} \\ 0 & \text{elsewhere.}\end{cases} \quad (3)$$

In Eq. (2), $E_y(x)$ is the electric field distribution in the vertical direction, ϵ_0 represents the dielectric constant, ω is the frequency of the propagating wave, and a_l the lth Fourier component of the tooth shape function. This calculation resulted in a value of 5 cm^{-1}, which is well within the range determined experimentally. Thus, there is no strong reason to believe that the grating strength is adversely affected by the compositional gradient we observed in the TEM study. By changing the sidewall angle of the individual grating teeth and preventing rounding of the profile, it should be possible to increase the grating coupling coefficient κ significantly and achieve a lower threshold current density for DFB lasers in this material system.

In conclusion, we have presented SEM and TEM micrographs along with x-ray data of third-order diffraction gratings in InGaN/GaN-based DFB lasers. We find that the tooth shape appeared different in the TEM versus SEM pictures because of a compositional gradient at the GaN/AlGaN interface, which caused much higher fringe contrast than obtainable from the actual GaN/AlGaN interface. Since such a compositional nonuniformity might affect DFB laser performance, we also compared numerically calculated and experimentally based values for the grating coupling coefficient, which indicated that the coupling coefficient is not significantly reduced by this compositional nonuniformity.

The authors are pleased to thank Fred Endicott and Brent Krusor for technical assistance. They also gratefully acknowledge helpful discussions with Thomas L. Paoli, Noble M. Johnson, Gary A. Evans (Southern Methodist University, Dallas, TX), and Peter S. Zory (University of Florida, Gainesville, FL). The work was supported partially by the Defense Advanced Research Projects Agency (DARPA Contract No. MDA 972-96-3-0014), and the Swiss National Science Foundation.

[1] S. Nakamura, M. Senoh, S. Nagahama, N. Iwasa, T. Yamada, T. Matsushita, Y. Sugimoto, and H. Kiyoku, Appl. Phys. Lett. **72**, 211 (1998).
[2] S. T. Kim, H. Amano, and I. Akasaki, Appl. Phys. Lett. **67**, 267 (1995).
[3] G. E. Bulman, K. Doverspike, S. T. Sheppard, T. W. Weeks, M. Leonard, H. S. Kong, H. Dieringer, J. Edmond, Y.-K. Song, M. Kuball, and A. V. Nurmikko, Appl. Phys. Lett. **72**, 1418 (1998).
[4] M. P. Mack, A. Abare, M. Aizcorbe, P. Kozodoy, S. Keller, U. K. Mishra, L. A. Coldren, and S. DenBaars, MRS Internet J. Nitride Semicond. Res. **2**, 41 (1997).
[5] D. P. Bour, M. Kneissl, L. T. Romano, M. D. McCluskey, C. G. Van de Walle, B. S. Krusor, R. M. Donaldson, J. Walker, C. J. Dunnrowicz, and N. M. Johnson, IEEE J. Sel. Top. Quantum Electron. **4**, 498 (1998).
[6] D. Hofstetter, R. L. Thornton, L. T. Romano, D. P. Bour, M. Kneissl, and R. M. Donaldson, Appl. Phys. Lett. **73**, 2158 (1998).
[7] L. T. Romano, B. S. Krusor, M. D. McCluskey, and D. P. Bour, Appl. Phys. Lett. **73**, 1757 (1998).
[8] S. N. G. Chu, T. Tanbun-Ek, R. A. Logan, J. Vandenberg, P. F. Sciortino, Jr., P. Wisk, and T. L. Pernell, IEEE J. Sel. Top. Quantum Electron. **3**, 862 (1997).
[9] G. Biasiol, E. Kapon, Y. Ducommun, and A. Gustafsson, Phys. Rev. B **57**, R9416 (1998).
[10] M. Walther, E. Kapon, C. Caneau, D. M. Hwang, and L. M. Schiavone, Appl. Phys. Lett. **62**, 2170 (1993).
[11] A. Yariv, *Quantum Electronics*, 2nd ed. (Wiley & Sons, New York, 1975), Chap. 19, pp. 515–533.
[12] M. Kneissl, D. P. Bour, N. M. Johnson, L. T. Romano, B. S. Krusor, R. Donaldson, J. Walker, and C. Dunnrowicz, Appl. Phys. Lett. **72**, 1539 (1998).
[13] M. Kneissl, D. Hofstetter, D. P. Bour, R. Donaldson, J. Walker, and N. M. Johnson, J. Cryst. Growth **189**, 846 (1998).

Downloaded 23 Dec 2005 to 134.121.128.99. Redistribution subject to AIP license or copyright, see http://apl.aip.org/apl/copyright.jsp